Scientific Reports

https://doi.org/10.1038/s41598-026-35455-z

Article in Press

Trend prediction method for capacitive voltage transformer measurement deterioration based on double Gaussian model-KAN fusion

Received: 26 January 2025

Accepted: 6 January 2026

Published online: 02 March 2026

Cite this article as: Du B., Diao Y., Zhou F. *et al.* Trend prediction method for capacitive voltage transformer measurement deterioration based on double Gaussian model-KAN fusion. *Sci Rep* (2026). https://doi.org/10.1038/s41598-026-35455-z

Bolun Du, Yinglong Diao, Feng Zhou, Xiaodong Yin & Shuai Yang

Trend prediction method for capacitive voltage transformer measurement deterioration based on double Gaussian model-KAN fusion

Bolun Du[1,*], Yinglong Diao[1,*], Feng Zhou[1], Xiaodong Yin[1], Yang Shuai[2]
[1]China Electric Power Research Institute, Wuhan 430074, China. [2]State Grid Hunan Electric Power Co., Ltd., Hunan 431000, China.
*email: bolundu93@163.com; diaoyinglong@epri.sgcc.com.cn

a trend prediction method for CVT measurement deterioration based on double Gaussian model-KAN fusion

***Abstract*: Capacitive voltage transformer (CVT) is an essential power measurement equipment in the power grid, which generates errors in long-term operation. Therefore, it is necessary to quantify the measurement performance of CVT and predict its measurement deterioration trend. This study proposes a measurement performance index to characterize the ratio error of CVT and a trend prediction method for CVT measurement deterioration based on double Gaussian model-KAN fusion. First, approximation and detail coefficients are formed after multilayer wavelet transform on the secondary side voltage of CVT. The maximum approximate coefficient is selected from the approximate coefficients, and the State of Performance (SOP) representation ratio error of CVT is calculated using the maximum approximate coefficient. Then, a Variational Modal Decomposition Mean Difference (VMD-MD) method is proposed to decompose the SOP sequence of CVT in multiple layers. The residual decomposed from the SOP sequence is used to characterize the deterioration trend of SOP, and the double Gaussian model is used to model and predict it. The Intrinsic Mode Functions (IMFs) decomposed from the SOP sequence are used to characterize the deterioration fluctuation of SOP, and the KAN algorithm is used to predict it. Finally, all the predicted results are added to represent the deterioration trend of CVT. Using CVTs and SWCVT-3 CVT online test system of China Electric Power Research Institute, the three-phase voltage data with increasing ratio error are collected, and the proposed double Gaussian model-KAN fusion method is tested. During the experiment, the ratio error of CVT was characterized effectively by SOP, and the proposed double Gaussian model-KAN fusion method could accurately predict the CVT SOP deterioration trend.**

***Keywords*: Capacitive voltage transformer, Ratio error, State of Performance, Double Gaussian model-KAN fusion**

I. Introduction

The voltage transformer is a device used to step down high voltage to low voltage, primarily for measurement and protection purposes in power systems [1]. In the field of voltage sensing, inductive voltage transformer (IVT) and capacitive voltage transformer (CVT) are common types of metering devices with distinct structural designs. The IVT operates based on the principle of electromagnetic induction. It features a simple structure and excellent transient response, making it particularly suitable for medium- and low-voltage distribution systems and high-precision metering applications [2]. In contrast, the CVT employs a combined structure of capacitive voltage division and electromagnetic conversion, making it better suited for high-voltage environments [3]. Traditional electromagnetic solutions face engineering challenges such as complex insulation design, increased physical size, and significantly higher manufacturing costs. Additionally, the potential for ferromagnetic resonance caused by core saturation poses a risk to system stability [4]. In this context, capacitive voltage transformers enable flexible regulation of primary voltage through capacitive division. They not only offer better insulation adaptability and cost-effectiveness but are also structurally designed to prevent ferromagnetic resonance. However, during long-term operation, factors such as ambient temperature can affect the stability of the internal capacitor divider, thereby impairing CVTs performance [5]. When the ratio error of CVTs exceeds the acceptable range, the secondary-side voltage may deviate significantly from the actual primary-side voltage, leading to inaccurate measurements [6]. Therefore, quantifying CVTs performance and accurately predicting the deterioration of its key indicators are essential to predictive maintenance, enhanced grid intelligence, and long-term system stability.

The most widely used technique for calibrating ratio errors in power grids employs standard CVT equipment during periodic outage verifications. According to national metrological regulations, CVTs

should be tested every four years; however, practical challenges such as difficulties in coordinating on-site power outage plans, limited detection time windows, and the bulkiness of testing and lifting equipment frequently lead to delays in these assessments [7]. Consequently, it is difficult to identify ratio errors in a timely manner during equipment operation, which can readily result in transaction disputes [8]. In response, researchers have proposed several methods for identifying CVT errors, primarily categorized into mechanism models and data-driven models. In the realm of mechanism modeling, Zhang et al. established a metrological model based on information-physical correlation analysis by considering the coupling and physical characteristics among the three-phase secondary voltages [9]. While this method meets the 0.2-level accuracy requirement, its demand for a high degree of three-phase load balance makes it susceptible to misjudging CVT measurement errors during long-term ratio difference monitoring. Alternatively, equivalent circuit models have been developed based on the insulation characteristics of the capacitive voltage divider and the electrical theory of CVT design to achieve precise ratio difference estimation [10, 11]. Nevertheless, slight variations in internal components like capacitors and reactors can significantly impact the parameter determination in these equivalent circuit models [12]. It is also important to note that these studies are primarily validated under simulation conditions, whereas in actual substation operations, factors such as electric field interference and load variations can compromise the accuracy of the equivalent circuit models [13]. On the other hand, the data-driven approach utilizes machine learning on measured data to construct black-box models for performance prediction. Many studies have treated the CVT degradation process as a spatiotemporal evolutionary process and have employed machine learning methods for forecasting [14-17]. For instance, Liu proposed support vector regression for power plant equipment fault prediction [15], Sun presented convolutional-recurrent neural networks for predicting power equipment performance [16], and Wang proposed maintenance prediction for high-speed railway power equipment using a long short-term memory recurrent neural network [17]. A common challenge for data-driven methods is their difficulty in learning from fluctuating and noisy measurement data. Furthermore, PCA has been particularly popular [18], with numerous studies focusing on its improvement—examples include replacing traditional statistical indicators with local outlier factors [19], adopting a sliding window approach with PCA [20], or calculating the Q value through independent component analysis [21]. However, these derived indicators cannot be directly applied to characterize the CVT ratio error. Simultaneously, the voltage measurement data from CVTs exhibits significant uncertainty and considerable fluctuation due to influences from the primary side voltage, load interference, and noise. This inherent variability complicates analysis, rendering the direct prediction of the CVT's deterioration trend a challenging task that has yet to be adequately addressed in existing research.

Wavelet transform is a localized analysis method of signal time and frequency. It gradually refines the signal into multi-scale detail coefficients and approximate coefficients by stretching and translating operations, which can focus on any detail of the signal and strip away random errors in the signal [22]. Gaussian model is a probabilistic model widely used in statistics and data analysis; it is based on normal distribution and is used to describe and predict the distribution of continuous random variables [23]. The Kolmogorov-Arnold Network (KAN) is a novel neural network architecture; unlike the traditional multilayer perceptron architecture, it can use fewer parameters to perform well in function fitting, state estimation and lifetime prediction, and the method is interpretable [24].

In this research, a measurement performance index is designed to characterize the ratio error of CVT, and a trend prediction method for CVT measurement deterioration based on double Gaussian model-KAN fusion is proposed. The collected secondary voltage of CVT is decomposed by wavelet transform. Approximation coefficients and detail coefficients are formed after multilayer wavelet decomposition. The maximum approximate coefficient is selected from the approximate coefficients, and the State of Performance (SOP) representing the ratio error of CVT is calculated using the maximum approximate coefficient. The Variational Modal Decomposition Mean Difference (VMD-MD) method is proposed to perform multi-layer decomposition on the SOP sequence. The decomposed residual of the SOP sequence can characterize the deterioration trend of SOP, and the double Gaussian model is used for modeling and predicting the residual. The decomposed IMFs of the SOP sequence can characterize the deterioration fluctuation of SOP, and the KAN algorithm is used for predicting IMFs. The two prediction models are combined to characterize the deterioration trend of SOP. Finally, the proposed CVT measurement deterioration trend prediction method is tested by CVTs and the SWCVT-3 CVT online test system of china electric power research institute. In the test, the calculated SOP sequence can represent the process of CVT measurement deterioration, and the double Gaussian model-KAN

fusion method can accurately predict the SOP deterioration trend of CVT.

The structure of this paper is organized as follows. Section II introduces the concept of CVT ratio error and the gradual degradation experiment. Section III presents the definition of the CVT performance index. Section IV describes the VMD-MD decomposition framework. Section V elaborates on the theoretical foundation of the prediction model. Section VI provides a detailed analysis of the experimental results. Finally, Section VII summarizes the contributions of this work.

II. CVT ratio error and gradual degradation experiment

A. CVT and ratio error

Fig. 1 depicts a CVT consisting of a capacitive voltage divider, a compensating inductor, and an intermediate voltage transformer. The capacitive voltage divider can be equivalent to a high-voltage capacitor C1 and a low-voltage capacitor C2, converting high voltage to medium voltage, whereas intermediate voltage transformer measures the voltage.

With the aging of CVT, the stability of three-phase voltage is affected. The ratio error reflects the difference between the actual rate of change and the rated rate of change. The ratio error e is the primary measurement error of CVT and can be defined as follows:

$$e=\frac{kV_s - V_f}{V_f} \times 100\% \qquad (1)$$

where V_s is the secondary voltage amplitude; V_f is the primary voltage amplitude; k is the rated ratio.

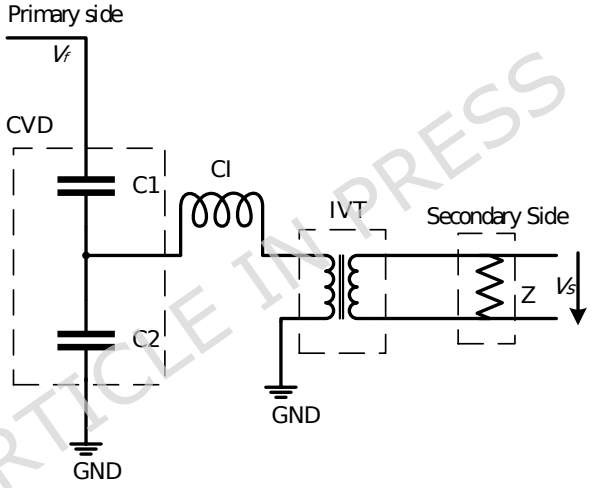

Fig. 1. Structure of CVT.

B. Data set

In order to verify the rigor and scientificity of the method proposed in this paper, a three-phase deterioration prediction experiment was performed for CVT based on the CVTs and the CVT online control system SWCVT-3 of china electric power research institute, as depicted in Fig. 2. The system includes a HEW99 full-function transformer calibrator and six voltage transformers. The output capacity of each phase of the system is 10 kVA, where the three phases are balanced. The device can set the ratio error of the secondary side of its own CVT and obtain the voltage data of the secondary side corresponding to the ratio error.

(a) (b)

Fig. 2. (a) CVTs and (b)the CVT online control system SWCVT-3 of china electric power research institute.

During the experiment, the ratio error of a certain phase was set to increase gradually, while the ratio error of the other two phases fluctuated in the normal range. An experiment was conducted in three phases: A, B, and C. The rated voltage of the primary side and the rated voltage of the secondary side of the CVT in the system were $100/\sqrt{3}$ kV and $100/\sqrt{3}$ V, respectively, and the three-phase signal frequency was 50 Hz.

The CVT deterioration experiment was conducted by gradually increasing the ratio error. Due to the limit setting of the control system, the differences between the initial ratio and termination ratio were found as -0.028% and 0.630% for phase A, whereas 0.127% and 0.789% for phase B, respectively. The initial ratio error and termination ratio error of phase C were -0.028% and 0.627%, respectively. Due to the interval constraint of the control system, a maximum of 36 samples with different ratio errors were collected in this period. Data were collected at one-second intervals, with each sample lasting 2 minutes, resulting in 120 data per sample. This experiment comprised a total of 4320 data.

Fig. 3 illustrates the three-phase voltage data collected from the three groups of degradation experiments. The voltage amplitude at which the CVT phase deteriorates exhibits an upward trend corresponding to an increase in error.

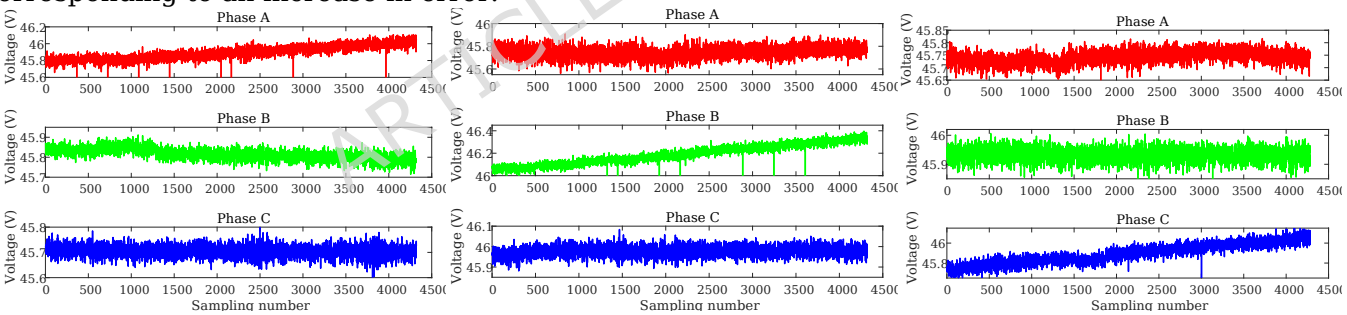

(a) (b)

(c)

Fig. 3. Three-phase voltage data collected from degradation experiments of (a) Degradation experiment 1 (b) Degradation experiment 2 (c) Degradation experiment 3.

III. Definition of the CVT performance index

Currently, there is no defined performance index for CVT. In addition, when CVT performance indicators are verified point by point, outliers can considerably influence the final evaluation. To address these issues, this study first employs wavelet transform as a preprocessing step. Through its multi-resolution analysis, the method effectively denoises the original signal and extracts stable low-frequency approximations. These approximations capture the core degradation trend and suppress high-frequency noise and local fluctuations, providing a cleaner signal representation. On this robust foundation, a SOP (CVT performance index) is defined to reliably characterize the CVT's degradation state.

Wavelet transform is an effective technique widely used in signal analysis. The wavelet transform formula is as follows:

$$a_{j+1}[m] = \sum_{k \in Z} h[k-2m]a_j[k] \qquad (2)$$

where $x[n]$is the measurement voltage signal measured on the secondary side; $a_j[k]$ is the approximation coefficient of the JTH layer, $h[k]$ is the wavelet function, and m is the index of the downsampling.

This paper applies wavelet transform for the first time, effectively extracting the main feature information while significantly reducing the data volume. This achieves the goal of minimizing memory usage and enhancing data processing efficiency. The wavelet transform is used to perform an i-level decomposition on $x[n]$ to obtain the approximate coefficient sequence. The approximation coefficient reflects the overall trend or low-frequency portion of the signal, representing the approximate shape or average behavior of the signal. To quantify the differences between the CVT output under different operating states and the reference state, this study uses the maximum approximation coefficients of the CVT in various states. It takes the maximum approximation coefficient of the CVT in the normal state as the reference to calculate the CVT measurement performance index, SOP. The specific calculation formula for SOP is as follows:

$$MAC_i = \max(a_i[1], a_i[2], \ldots . a_i[m]) \qquad (3)$$

$$SOP = \exp(-100 * \frac{MAC_i - MAC_0}{MAC_0}) \qquad (4)$$

where MAC_i represents the maximum approximation coefficient of the calculated test data; MAC_0 represents the maximum approximation coefficient of the normal state of CVT.

This paper decomposes 120 sample data with 36 error levels in four layers and calculates 36 sample data based on the above formula. The 36 samples data with different error levels are evenly divided into training and test data, each comprising 18 samples. Among them, a prediction model is established based on the training set and the already trained model is verified based on the test set. The SOPs for the A, B, and C phases of CVT are calculated according to Equ. (4), as shown in Fig. 4. In Fig. 4, as the ratio error increases, the SOP of CVT exhibits a downward trend. This phenomenon indicates that SOP can sensitively capture the performance degradation of the CVT under significant errors and intuitively reveal the decline in its stability and accuracy. Thus, the proposed SOP can effectively characterize the ratio error of CVT.

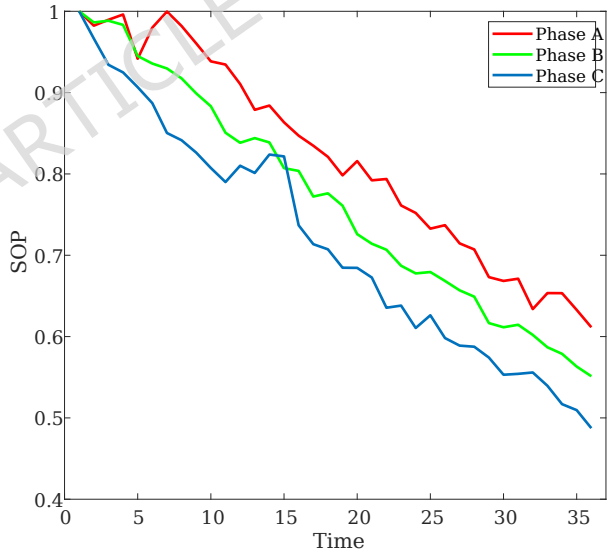

Fig. 4. SOPs for the A, B, and C phases of CVT.

IV. VMD-MD signal decomposition method

Although the wavelet-derived SOP sequence reflects the core degradation trend, it may still contain residual medium-to-low frequency fluctuations caused by disturbances from the primary voltage of the power grid and measurement inaccuracies. To further separate these multi-scale components for refined modeling, the SOP sequence is decomposed into multiple IMFs with well-defined frequency contents using the VMD-MD method. This secondary decomposition lays a solid foundation for constructing customized prediction models for different IMFs, thereby enhancing the accuracy of

CVT degradation trend prediction.

VMD algorithm is a signal processing method that adaptively decomposes the SOP sequence into a mode set $u_k(k=1,\mathrm{K},K)$ with different center frequency w_k. It transforms decomposition into two detailed processes of constructing and solving variational agents.

Step 1: Calculate the unilateral spectrum of each mode through the Hilbert transform, and the unilateral spectrum $z_k(t)$ is expressed as

$$z_k(t)=(d(t)+\frac{j}{pt})u_k(t) \tag{5}$$

where $d(t)$ is an impulse function; t is a time index; j is an imaginary number unit.

Step 2: Modulate the spectrum of each mode into the response frequency range

$$S_k(w)=[(d(t)+\frac{j}{pt})u_k(t)]e^{-jw_kt} \tag{6}$$

Step 3: Construct the constrained variational problem

$$\begin{cases} f(u_k,w_k)=\min\limits_{\{u_k\}\{w_k\}}\left\{\sum\limits_K\left\|\P_t[((d(t)+\frac{j}{pt})u_k(t)e^{-jw_kt}]\right\|_2^2\right\} \\ s.t.\sum\limits_K u_k=SOP \end{cases} \tag{7}$$

where $\{u_k\}=\{u_1,\mathrm{K},u_k\}$ represents the amplitude of modal component; $\{w_k\}=\{w_1,\mathrm{K},w_k\}$ represents the frequency center of the modal component; $\P_t$ represents the partial derivative concerning t; K is the number of modal components; $S_k(w)$ represents the unilateral spectrum corresponding to the KTH modal component, and $f()$ is the constructed cost function.

To resolve the variational problem, the Lagrange multiplier l and quadratic penalty factor a are introduced to transform the constrained variational problem into an unconstrained variational problem. Augmented Lagrange is described as follows:

$$L(\{u_k\},\{w_k\},l)=a\sum_K\left\|\P_t[((d(t)+\frac{j}{pt})u_k(t)e^{-jw_kt}]\right\|_2^2+\left\|f(t)-\sum_K u_k(t)\right\|_2^2+\langle l(t),SOP(t)-\sum_K u_k(t)\rangle \tag{8}$$

The specific number of decomposition levels is crucial for achieving optimal decomposition results. For instance, if the number of decomposition levels is too small, it will be difficult to extract meaningful multi-scale features. Here, the number of decomposition layers of the VMD method needs to be determined. The VMD algorithm introducing Mean difference (MD) to determine the decomposition layer is called the VMD-MD algorithm.

Step 4: This paper optimizes the Lagrange function using the substitution direction multiplier method and iteratively updates the modal frequency and amplitude until the decomposition threshold is reached.

The MD calculation is as follows:

$$MD_h=\sum_{i=1}^{n}\left|R_i^h-R_i^{h-1}\right| \tag{9}$$

where h represents the number of layers in the variational mode decomposition, and $R^h{}_i$ is the residual of the SOP sequence obtained by decomposing the h layer, representing the number of decomposition layers. The residual term usually retains the low-frequency components in the signal and reveals the global trend of the SOP over time or the degradation process of the health state. MD is the average difference in the decomposition times of two adjacent layers; n is the length of the residual of the decomposition, i.e., the number of elements. When the average difference change after the decomposition of the K layer tends to be stable, it is considered that the current decomposition times are the optimal value.

When decomposition layer h=1, the current residual is calculated with the original signal. For k >1, the MD of the decomposed residual is calculated with the last decomposed residual. When MD is lower than the threshold, the residual is considered to have little change, decomposition is terminated, and the layer is determined.

In this paper, the decomposition threshold is set to 0.001, and the number of decomposition layers is determined by the MD algorithm. The SOP sequence decomposition is executed using VMD-MD, with a threshold set at 1×10^{-4}. The threshold is surpassed during decomposition when reaching the 7th layer, as illustrated in Table I. It is manifested that the SOP of the A, B, and C phases need to be decomposed to the 6th layer.

TABLE I

MEAN DIFFERENCE OF THE RESIDUAL OF VMD-MD DECOMPOSITION CORRESPONDING TO DIFFERENT H

Layer	Phase A	Phase B	Phase C
1	1.382×10^{-3}	1.510×10^{-3}	5.962×10^{-4}
2	6.985×10^{-3}	5.006×10^{-3}	7.092×10^{-3}
3	4.096×10^{-4}	3.14×10^{-3}	5.576×10^{-3}
4	8.276×10^{-4}	6.814×10^{-4}	5.507×10^{-4}
5	1.933×10^{-4}	1.249×10^{-3}	5.643×10^{-4}
6	4.262×10^{-4}	1.988×10^{-4}	1.484×10^{-4}
7	8.563×10^{-5}	4.233×10^{-5}	8.791×10^{-5}

Additionally, the setting of the penalty factor α is also crucial. In this study, when determining the value of the penalty factor α, we followed the principle of retaining the maximum amount of effective information in the signal. We conducted multiple experiments within the range of 0.1 to 10 for α. Subsequently, we calculated the information retention rate of the residual signal relative to the original signal for each set of parameters and analyzed its variation trend. When the energy ratio showed a noticeable inflection point as α increased, we selected the α value at that inflection point as the final parameter setting. The inflection point typically represents a transition from “rapid change” to “gradual change” in the system, indicating that further increasing α no longer significantly enhances information retention. At this stage, the parameter setting becomes more representative and robust. For example, for the degraded part of phase A, the experimental results are shown in Figure 5, with the final α value set to 1. Similarly, using this method, the final α values for phases B and C under their respective degradation conditions were determined to be 2 and 1, respectively.

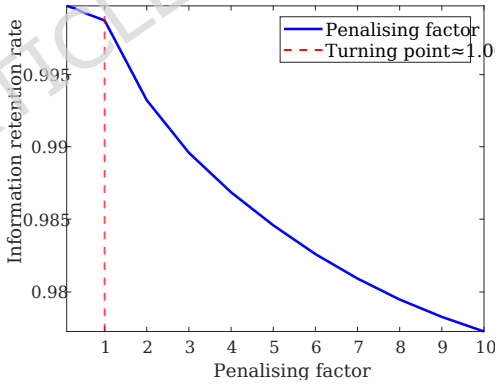

Fig. 5. α sets the experimental results.

The VMD-MD algorithm decomposes the CVT three-phase SOP respectively, yielding the results in Fig. 6. The residuals are close to the values of SOPs, which reflects the deterioration trend of SOPs. The IMFs show the characteristics of small value and strong fluctuation.

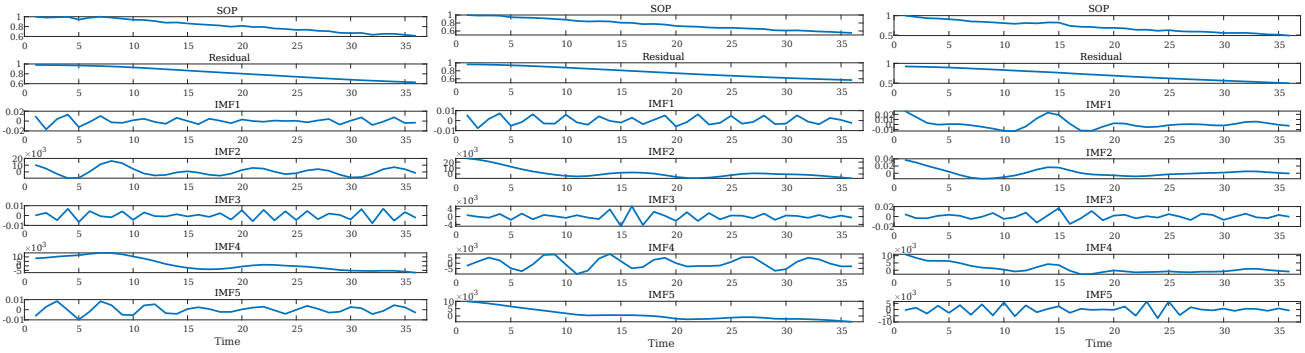

(a) (b) (c)

Fig. 6. SOP decomposition results of (a) Phase A (b) Phase B (c) Phase C.

V. SOP prediction model

A. Double Gaussian model

Under ideal conditions, without accounting for the introduction of noise, the secondary-side voltage exhibits a linear increase with the ratio difference. This relationship is determined jointly by the linear transmission characteristics of the transformer and the definition of the ratio difference. However, in real working conditions, due to nonlinear, sudden changes and other factors, the degraded signal distribution is bimodal or multi-modal, which increases the difficulty of performance estimation. Therefore, this study proposed a double-Gaussian model to decompose complex data into two independent components and quantify the characteristics of each independent component by adjusting the parameters of the model to accurately fit the CVT deterioration trend. The working principle of the double Gaussian model is defined as follows:

$$Y = a_1 e^{-(x-b_1)/c_1} + a_2 e^{-(x-b_2)/c_2} \tag{10}$$

where Y is the target variable; x is the input feature; a_1 and a_2 are the amplitude of two independent components, respectively; b_1 and b_2 are the mean value of two independent components, respectively; c_1 and c_2 are the variance of two independent components, respectively.

B. KAN

The fundamental computational unit of a traditional multi-layer perceptron (MLP) is the neuron, which performs weighted summation of input signals followed by fixed, non-linear activation functions. The choice of activation function significantly influences the model's predictive capability. However, a key limitation of MLPs lies in their use of identical, static activation functions within each layer, which restricts the model's representational capacity and generalization ability when handling complex nonlinear relationships. Notably, KAN, grounded in the Kolmogorov-Arnold representation theorem, introduce a paradigm shift by replacing MLPs' static activation functions with parametric spline functions positioned on the network edges. This structural innovation enables dynamic and adaptive modeling of high-order nonlinear relationships, substantially enhancing the model's expressive power in complex function approximation tasks. A comparative visualization of KAN and MLP architectures is presented in Fig. 7. The Kolmogorov-Arnold framework operates through the following mechanism.

$$f(x) = f(x_1, x_2, \ldots, x_n) = \sum_{q=0}^{2n} \Phi_q \left(\sum_{p=1}^{n} \varphi_{q,p}(x_p) \right) \tag{11}$$

where x_p represents the p-th variable in the multivariable; q is the index of external functions; p is the dimension of the input vector; Φ is the combination of univariable functions; φ is the univariable function.

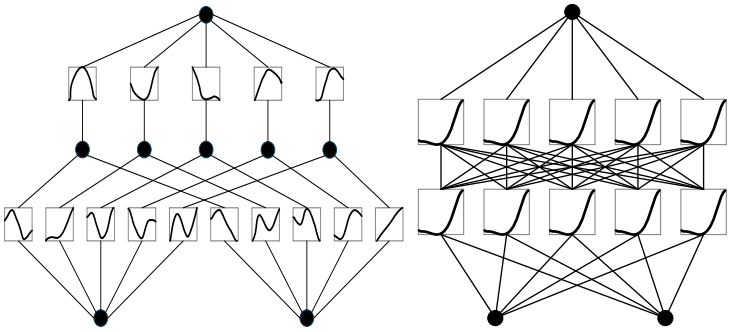

Fig. 7. Network structure of (a) KAN (b) MLP.

In this study, considering that the secondary-side voltage of the CVT is influenced by multiple factors such as load changes—which can compromise the accuracy of point-by-point detection—a constant time unit is adopted as the detection cycle. However, this approach significantly reduces the number of available data samples. KAN employs a learnable B-spline activation function that can dynamically adjust its shape based on the data, thereby enhancing the model's expressive power and adaptability. Furthermore, this learnable activation function can adaptively modulate the model complexity in response to limited data, enabling more accurate fitting of key features while avoiding overfitting. Under small sample conditions, this data-driven approach helps to extract features more efficiently, reduce overfitting, and improve robustness and generalization.

During the aging process of CVT, the calculated continuous SOP sequence often drops irregularly with large fluctuations. Thus, the VMD-MD method is used to decompose the SOP sequence of CVT in multiple layers. The degraded trend of the decomposed SOP sequence is modeled and predicted using the double Gaussian model. The fluctuation part of the decomposed SOP sequence is predicted by the KAN algorithm.

VI. Results and discussion

In this study, the Levenberg-Marquardt (LM) algorithm is used to optimize the parameters of the double Gaussian model to improve its fitting effect. Table II lists the parameters of the double Gaussian model in the three experiments. The RMSE, MAE, and R^2 values comparing the final predicted results to the actual values are presented in Table III. Fig. 8 depicts the predicted results using double Gaussian model. According to the experimental results in Table III and Fig. 8, RMSE and MAE are very small, and R^2 is greater than 0.99 and close to 1. Furthermore, to demonstrate the superiority of the proposed model, this paper compares it to the Gaussian model through a series of experiments. The prediction results clearly show that the DGM significantly outperforms the GM. This notable performance difference indicates that the residual terms during the gradual change process of the CVT error exhibit obvious multimodal distribution characteristics rather than a Gaussian distribution. The Gaussian model performs poorly because it fails to capture these multimodal characteristics in the residual distribution. In contrast, the GM model, by incorporating a mixture of two Gaussian components, can more accurately characterize the residual distribution at different degradation stages, thereby significantly improving prediction accuracy.

TABLE II
PARAMETERS OF DOUBLE GAUSSIAN MODEL

Layer	Pahse A	Pahse B	Pahse C
a_1	16.1395	-0.6361	-509.5130
b_1	-353.8699	-18.3374	-102.5601
c_1	-152.5579	9.4689	25.1578
a_2	-0.1459	154.410	50.7810

		0	
b_2	-4.3410	-570.8287	-384.0487
c_2	6.1070	-180.8143	137.8615

TABLE III
RMSE, MAE, AND R^2 OF PREDICTION

	DGM			GM		
	Pahse A	Pahse B	Pahse C	Pahse A	Pahse B	Pahse C
RMSE	0.0040769	0.0055827	0.0033573	0.0456612	0.0633772	0.0761982
MAE	0.0027978	0.0038658	0.0029801	0.0379002	0.0530958	0.0645704
R^2	0.99521	0.99048	0.99711	0.46487	-0.22646	-0.67372

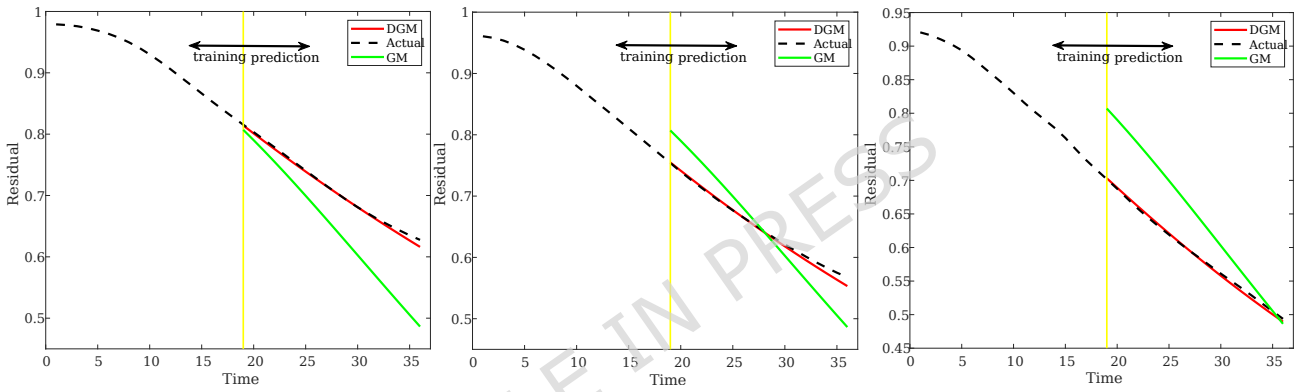

(a) (b)
(c)

Fig. 8. Prediction results of double Gaussian model of (a) Phase A (b) Phase B (c) Phase C.

The KAN method is used to predict the trend of the IMFs, i.e., the volatility signals of the CVT three-phase SOP sequence, and compared with the LSTM [25], GRU [26], Transformer [27] and SVR [28]. The final prediction results are shown in Fig. 9, Fig. 10, and Fig. 11, whereas the evaluation indicators of each prediction result are presented in Table IV, Table V, and Table VI, respectively. The IMFs of the three-phase SOP sequence change rapidly and irregularly, which increases the difficulty of prediction. However, KAN adds the working mode of "continual learning" in the connection part of neurons at each layer and realizes the automatic selection of activation functions using B-spline, enhancing the prediction ability of the KAN model in complex situations. By observing the experimental results in Figs. 9–11, and the performance indexes in Tables IV– VI, it was found that the overall prediction accuracy of KAN is relatively ideal in predicting IMFs. Consider the IMF prediction for phase A SOP as an example. During the prediction process, IMF1, IMF3, and IMF5 are relatively irregular. Each IMF has just 18 training samples. The comparison results of the final models indicate that the RMSE and MAE for IMF3 prediction using KAN are 0.0039267 and 0.0032691, respectively. Compared with SVR, LSTM, transformer and GRU, RMSE decreased by 0.0012371, 0.0009206, 0.0016518 and 0.0006357, whereas MAE decreased by 0.0009502, 0.0012599, 0.0012805, 0.0009506, respectively, further confirming the superiority and applicability of KAN method.

Many studies have verified the superiority of LSTM, transformer and GRU methods in time prediction series. However, most of the IMFs in the SOP sequence are characterized by high variation frequency, complexity, and small sample size, which leads to insufficient training of LSTM, transformer and GRU methods in experiments, limiting their effectiveness in IMF prediction in the SOP sequence. Although the superiority of SVR in small sample prediction has been proved, SVR fails

to capture the correlation features of data in time series space and has poor performance in time series prediction. Compared with the comparative methods, the KAN method improves the robustness and flexibility of the prediction due to its learnable activation function. Therefore, the KAN method can obtain more accurate predictions in complex decomposed signals.

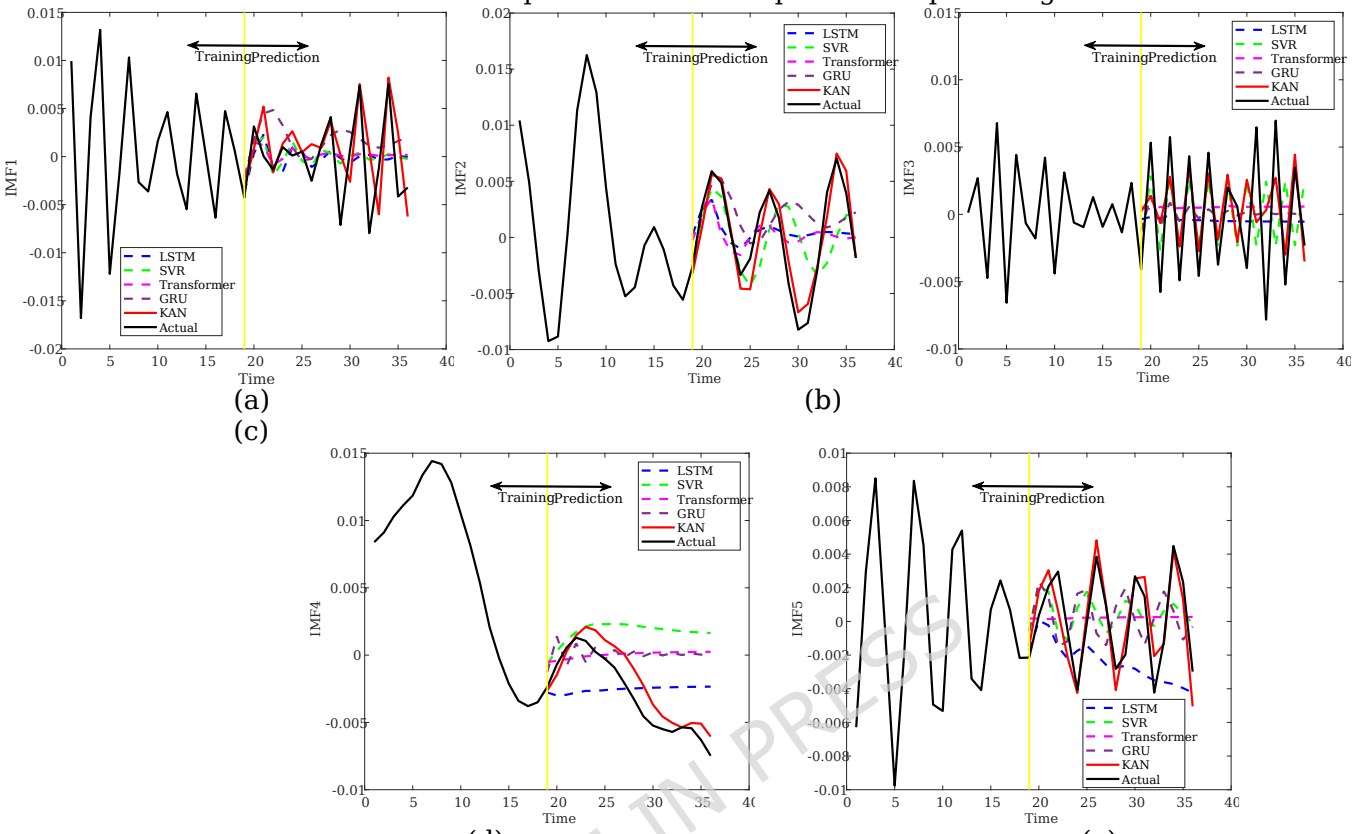

Fig. 9. (a)IMF1, (b)IMF2, (c)IMF3, (d)IMF4 and (e)IMF5 prediction results of Phase A SOP decomposition.

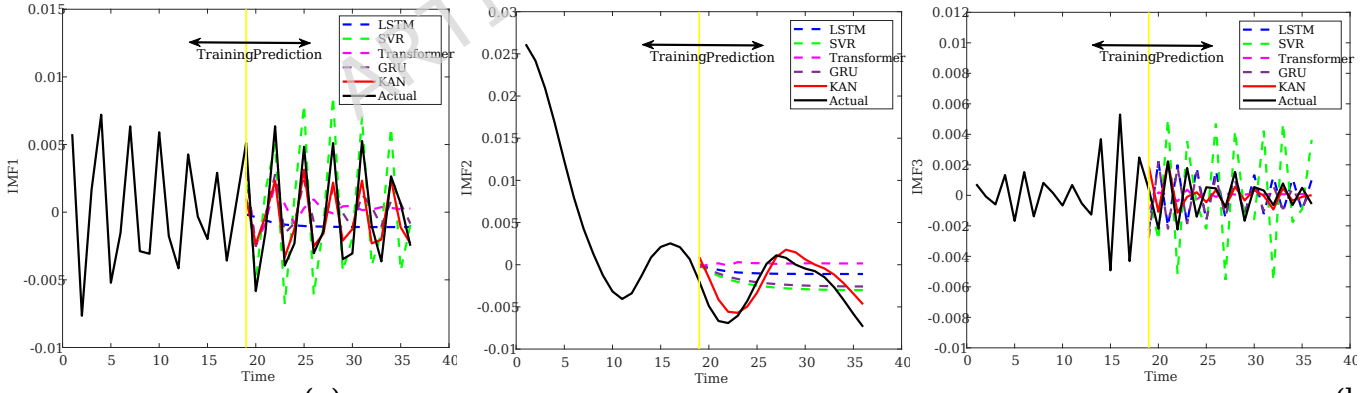

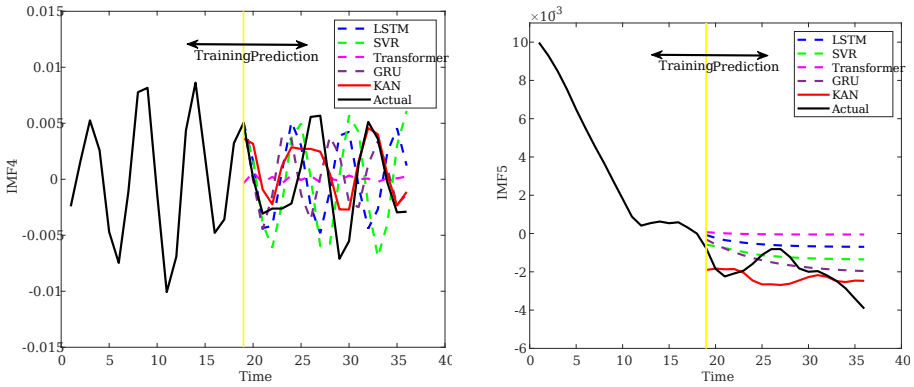

Fig. 10. (a)IMF1, (b)IMF2, (c)IMF3, (d)IMF4 and (e)IMF5 prediction results of Phase B SOP decomposition.

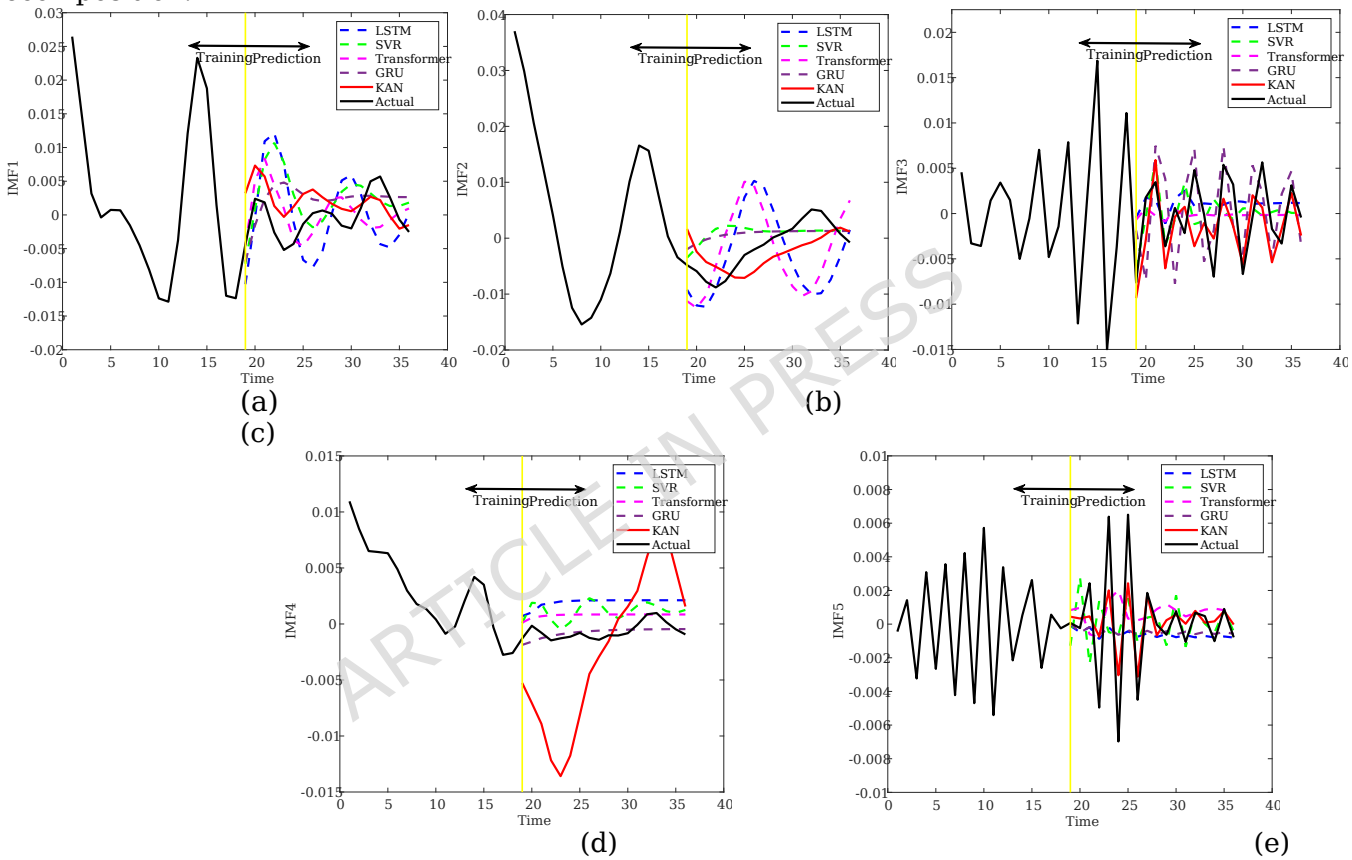

Fig. 11. (a)IMF1, (b)IMF2, (c)IMF3, (d)IMF4 and (e)IMF5 prediction results of Phase C SOP decomposition.

TABLE IV
PREDICTION RESULTS OF IMFS OF PHASE A SOP DECOMPOSITION USING DIFFERENT COMPARISON METHODS

		IMF1	IMF2	IMF3	IMF4	IMF5
SVR	RMSE	0.0037849	0.0041196	0.0051638	0.0054468	0.0026472
	MAE	0.0028749	0.0031559	0.0042193	0.0045992	0.0023683
LSTM	RMSE	0.0040638	0.0039943	0.0048473	0.0029695	0.0037235
	MAE	0.0030922	0.0033327	0.0045290	0.0026971	0.0028885
GRU	RMSE	0.0047157	0.0047321	0.0045624	0.0040757	0.0033087
	MAE	0.0037927	0.0036328	0.0042197	0.0033181	0.0030212
Transformer	RMSE	0.0039943	0.0039875	0.0049209	0.0041490	0.0026520
	MAE	0.0030145	0.0033599	0.0045496	0.0033338	0.0022970

KAN	RMSE	0.0038844	0.0014297	0.0039267	0.0013138	0.0012210
	MAE	0.0028332	0.0011624	0.0032691	0.0011096	0.0010051

TABLE V
PREDICTION RESULTS OF IMFS OF PHASE B SOP DECOMPOSITION USING DIFFERENT COMPARISON METHODS

		IMF1	IMF2	IMF3	IMF4	IMF5
SVR	RMSE	0.002616	0.0031670	0.0029553	0.0064210	0.0011341
	MAE	0.0023293	0.0028225	0.0025438	0.0053709	0.0009154
LSTM	RMSE	0.0038949	0.0035039	0.0024869	0.0061406	0.0016039
	MAE	0.0032081	0.0028449	0.0021036	0.0049248	0.0013985
GRU	RMSE	0.0024267	0.0032173	0.0024107	0.0044098	0.0009029
	MAE	0.0021857	0.0027905	0.0019528	0.0033717	0.0007410
Transformer	RMSE	0.0033970	0.0041512	0.0012395	0.0038420	0.0020910
	MAE	0.0030551	0.0032777	0.0010648	0.0032821	0.0019208
KAN	RMSE	0.0021212	0.0017731	0.0009338	0.0024708	0.0009738
	MAE	0.0017226	0.0015411	0.0007380	0.0020059	0.0007381

TABLE VI
PREDICTION RESULTS OF IMFS OF PHASE C SOP DECOMPOSITION USING DIFFERENT COMPARISON METHODS

		IMF1	IMF2	IMF3	IMF4	IMF5
SVR	RMSE	0.0056801	0.0048886	0.0041592	0.0019559	0.0033528
	MAE	0.0043343	0.0037588	0.0033646	0.0017981	0.0023593
LSTM	RMSE	0.0073289	0.0084064	0.0041394	0.0027020	0.0031877
	MAE	0.0063184	0.0071461	0.0034149	0.0025907	0.0022349
GRU	RMSE	0.004505	0.0044182	0.0050743	0.0007182	0.0032036
	MAE	0.0036962	0.0035555	0.0046165	0.0005936	0.0022342
Transformer	RMSE	0.0042280	0.0087652	0.0039821	0.0016017	0.0034102
	MAE	0.0035437	0.0077947	0.0032130	0.0014531	0.0024282
KAN	RMSE	0.0036963	0.0037606	0.0035190	0.0065644	0.0021060
	MAE	0.0032588	0.0035555	0.0029785	0.0055952	0.0014658

The residual prediction results based on the double Gaussian model (DGM) and the IMFs prediction results obtained from the KAN, LSTM, GRU, and SVM methods are superimposed to produce overall prediction results of the SOP sequence, as illustrated in Fig. 12. The result evaluation indicators of the predictions are presented in Table VII. At the same time, in order to highlight the superiority of the proposed method, the true and predicted values of each model under phase A degradation conditions are shown in Table VIII. The double Gaussian model-KAN fusion method yields the best prediction effect in the three-phase deterioration experiments. For example, the experimental results of phase A deterioration, the RMSE, MAE, and R2 of the double Gaussian model-KAN fusion prediction results are 0.00863, 0.0066781, and 0.98108, respectively. Compared with the experimental results of SVR, LSTM, transformer and GRU methods combined with the double Gaussian model, the corresponding RMSE decreased by 0.002238, 0.00347, 0.00277, and 0.003149, respectively, and MAE decreased by 0.0017093, 0.0034869, 0.0020219 and 0.0021796 respectively. Furthermore, R2 for SVR, LSTM, transformer and GRU methods increased by 0.01108, 0.01828, 0.01408, and 0.01633, respectively. Based on the above, this paper uses the Wasserstein distance as the performance metric to fit the statistical model to the data, and the fitting effect is analyzed through statistical tests. The corresponding results for the deterioration of phases A, B, and C are 0.0028842475842130568, 0.0040461435116515305, and 0.0030781255932507234, respectively. These relatively small values of the Wasserstein distance under the three-phase deterioration conditions indicate that the constructed statistical model can more accurately fit the original data distribution, demonstrating good modeling accuracy and generalization ability. The overall SOP prediction results further proved that the KAN method determines the activation function through "continual learning," which can effectively capture key features in the data, robustness to noise and outliers, performing well in small sample data tasks when dealing with complex signals.

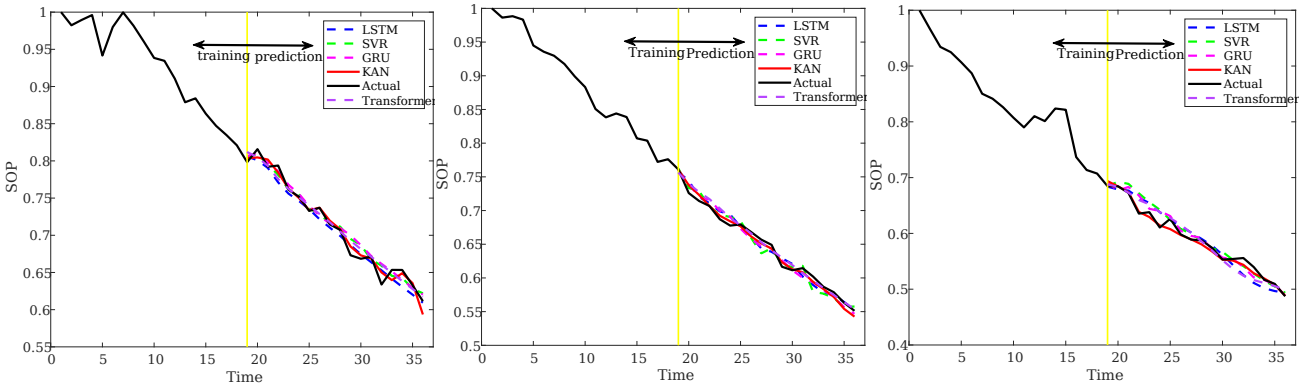

Fig. 12. Overall prediction results of CVT SOP of (a) Phase A, (b) Phase B and (c) Phase C

TABLE VII
PREDICTION RESULTS OF THREE PHASES' SOPS USING DIFFERENT COMPARISON METHODS

		Phase A	Phase B	Phase C
DGM-SVR	RMSE	0.010868	0.010065	0.014517
	MAE	0.0083874	0.0081963	0.010489
	R^2	0.97	0.97021	0.93663
DGM-LSTM	RMSE	0.0121	0.0099898	0.016092
	MAE	0.010165	0.0086675	0.012887
	R^2	0.9628	0.97065	0.92213
DGM-GRU	RMSE	0.011779	0.0088777	0.012786
	MAE	0.0088577	0.0079256	0.0088499
	R^2	0.96475	0.97682	0.95084
DGM-Transformer	RMSE	0.0114	0.0095	0.0151
	MAE	0.0087	0.0081	0.0113
	R^2	0.9670	0.9706	0.9318
DGM-KAN	RMSE	0.00863	0.0065031	0.0071273
	MAE	0.0066781	0.0057438	0.0050522
	R^2	0.98108	0.98756	0.98472

TABLE VIII
THE TRUE VALUE AND THE PREDICTED VALUE OF EACH MODEL FOR A PHASE.

Model	DGM-SVR	DGM-LSTM	DGM-GRU	DGM-Transformer	DGM-KAN	Actual
Sample1	0.803720	0.805730	0.806525	0.811936	0.803696	0.798261
Sample2	0.809447	0.800932	0.810172	0.804958	0.804648	0.815810
Sample3	0.794974	0.790590	0.797464	0.793419	0.80184	0.792132
Sample4	0.781315	0.771144	0.786121	0.775541	0.784303	0.793772
Sample5	0.761658	0.756008	0.767894	0.762414	0.762857	0.761236

VII. Conclusion

This study proposed a double Gaussian model-KAN fusion method to address the problem of CVT measurement deterioration prediction. The key contributions of this research are outlined as follows:

(1) A measurement performance index, SOP, was presented to characterize CVT ratio error. The CVT secondary voltage was decomposed by wavelet transform, and the maximum approximate coefficient was selected from the approximate coefficients. The SOP of CVT was calculated using the maximum approximate coefficient, which can demonstrate the CVT measurement of the deterioration process.

(2) The VMD-MD method was proposed to decompose the SOP sequence, and the double Gaussian model-KAN fusion was presented to predict the SOP deterioration process. The decomposed residual

could be used to characterize the deterioration trend of SOP, and the double Gaussian model was used for modeling and predicting it. The decomposed IMF could be used to characterize the deterioration fluctuation of SOP, and the KAN algorithm was used to predict it. The deterioration trend of SOP was generated by summarizing the results of the two predictions.

(3) The CVTs and SWCVT-3 CVT online test system of china electric power research institute were used to verify the proposed method. During the experiment, the proposed SOP could characterize the ratio error. Thus, the proposed double Gaussian model-KAN fusion method can produce a better effect than comparative methods.

References

[1] Ushakov V Y, Mytnikov A V, Rakhmonov I U. High-voltage equipment of power systems[J]. Power systems. Springer, Cham. https://doi. org/10.1007/978-3-031-38252-9, 2023.

[2] Beheshti Asl M, Fofana I, Meghnefi F. Review of various sensor technologies in monitoring the condition of power transformers[J]. Energies, 2024, 17(14): 3533.

[3] Faifer M, Toscani S, Ottoboni R. Electronic combined transformer for power-quality measurements in high-voltage systems[J]. IEEE Transactions on instrumentation and measurement, 2011, 60(6): 2007-2013.

[4] Borghei M, Ghassemi M. Insulation materials and systems for more-and all-electric aircraft: A review identifying challenges and future research needs[J]. IEEE Transactions on Transportation Electrification, 2021, 7(3): 1930-1953.

[5] Zhang Y, Zhang C, Li H, et al. An online detection method for capacitor voltage transformer with excessive measurement error based on multi-source heterogeneous data fusion[J]. Measurement, 2022, 187: 110262.

[6] Ameli A, Ghafouri M, Salama M M A, et al. An auxiliary framework to mitigate measurement inaccuracies caused by capacitive voltage transformers[J]. IEEE Transactions on Instrumentation and Measurement, 2022, 71: 1-11.

[7] Zhou F, Zhao P, Lei M, et al. Capacitive voltage transformer measurement error prediction by improved long short-term memory neural network[J]. Energy Reports, 2022, 8: 1011-1021.

[8] Li Z, Li Q, Wu Z, et al. Research into an online calibration system for the errors of voltage transformers based on open–closed capacitor[J]. Energies, 2018, 11(6): 1455.

[9] Zhang Z, Li H, Tang D, et al. Monitoring the metering performance of an electronic voltage transformer on-line based on cyber-physics correlation analysis[J]. Measurement Science and Technology, 2017, 28(10): 105015.

[10] Chen B, Du L, Liu K, et al. Measurement error estimation for capacitive voltage transformer by insulation parameters[J]. Energies, 2017, 10(3): 357.

[11] Freiburg M, Sperling E, Predl F. Capacitive voltage transformers-electrical performance and effective diagnostic measures[C]//2016 International Conference on Condition Monitoring and Diagnosis (CMD). IEEE, 2016: 20-23.

[12] de Andrade Reis R L, Neves W L A, Lopes F V. Coupling capacitor voltage transformers models and impacts on electric power systems: A review[J]. IEEE Transactions on Power Delivery, 2019, 34(5): 1874-1884.

[13] Meng Z, Li H, Zhang C, et al. Research on the reliability of capacitor voltage transformers calibration results[J]. Measurement, 2019, 146: 770-779.

[14] Zhang W, Shi Y, Yu J, et al. Online measurement of capacitor voltage transformer metering errors based on GRU and MTL[J]. Electric Power Systems Research, 2023, 221: 109473.

[15] Liu J, Geng G. Fault prediction for power plant equipment based on support vector regression[C]//2015 8th International Symposium on Computational Intelligence and Design (ISCID). IEEE, 2015, 2: 461-464.

[16] Sun L, Liu T, Xie Y, et al. Real-time power prediction approach for turbine using deep learning techniques[J]. Energy, 2021, 233: 121130.

[17] Wang Q, Bu S, He Z. Achieving predictive and proactive maintenance for high-speed railway power equipment with LSTM-RNN[J]. IEEE Transactions on Industrial Informatics, 2020, 16(10): 6509-6517.

[18] Zhang C, Meng Z, Chen M, et al. Monitoring the ratio error drift of CVTs connected to the same phase along with KDE-PCA[C]//2019 IEEE International Instrumentation and Measurement Technology Conference (I2MTC). IEEE, 2019: 1-6.

[19] Zhao X, Wei H. Error Evaluation Method of Capacitive Voltage Transformer Based on Improved Principal Component Analysis[C]//Journal of Physics: Conference Series. IOP Publishing, 2023, 2625(1): 012041.

[20] Zhang Z, Chen Q, Hu C, et al. Evaluating the metering error of electronic transformers on-line based on vn-mwpca[J]. Measurement, 2018, 130: 1-7.

[21] Zhang C, Li H, Chen Q. Detection of the ratio error drift in CVT considering AVC[J]. Measurement, 2019, 138: 425-432.

[22] Zhang C, He Y, Yang T, et al. An analog circuit fault diagnosis approach based on improved wavelet transform and MKELM[J]. Circuits, Systems, and Signal Processing, 2022: 1-32.

[23] Bakka H, Vanhatalo J, Illian J B, et al. Non-stationary Gaussian models with physical barriers[J]. Spatial statistics, 2019, 29: 268-288.

[24] Vaca-Rubio C J, Blanco L, Pereira R, et al. Kolmogorov-arnold networks (kans) for time series analysis[J]. arxiv preprint arxiv:2405.08790, 2024.

[25] Zhao S, Zhang C, Wang Y. Lithium-ion battery capacity and remaining useful life prediction using board learning system and long short-term memory neural network[J]. Journal of Energy Storage, 2022, 52: 104901.

[26] Zhang C, Luo L, Yang Z, et al. Battery SOH estimation method based on gradual decreasing current, double correlation analysis and GRU[J]. Green Energy and Intelligent Transportation, 2023, 2(5): 100108.

[27] Hu, Wangyang, et al. "Integrated Method of Future Capacity and RUL Prediction for Lithium-Ion Batteries Based on CEEMD-Transformer-LSTM Model." Energy Science & Engineering 12.11 (2024): 5272-5286.

[28] Azimi-Pour M, Eskandari-Naddaf H, Pakzad A. Linear and non-linear SVM prediction for fresh properties and compressive strength of high volume fly ash self-compacting concrete[J]. Construction and Building Materials, 2020, 230: 117021.

Acknowledgments

This study was partially supported by State Grid Science and Technology Project (5700-202422270A-1-1-ZN) and China Electric Power Research Institute-Fund Project (JL83-23-015)

Author contributions

This work was conceived by Bolun Du and Yinglong Diao. Data was collected and analyzed by Feng Zhou. Xiaodong Yin and Yang Shuai helped to revise manuscript and proposed constructive opinions. All authors contributed to the article and approved the submitted version.

Corresponding author

Correspondence to Bolun Du and Yinglong Diao.

Data availability statements

The datasets used and/or analysed during the current study available from the corresponding author on reasonable request.

Competing interests

The authors declare no competing interests.